PAPER

A 3D percolation model for multicomponent nanocarbon composites: the critical role of nematic transition

To cite this article: Xiaojuan Ni *et al* 2019 *Nanotechnology* **30** 185302

IOP Publishing Nanotechnology
Nanotechnology 30 (2019) 185302 (9pp) https://doi.org/10.1088/1361-6528/ab012f

A 3D percolation model for multicomponent nanocarbon composites: the critical role of nematic transition

Xiaojuan Ni[1], Chao Hui[2,3], Ninghai Su[2], Raymond Cutler[1,2] and Feng Liu[1,4]

[1] Department of Materials Science and Engineering, University of Utah, Salt Lake City, UT 84112, United States of America
[2] Life-E LLC, Salt Lake City, UT 84103, United States of America
[3] NaXi Research Center, Hebei Institute of Tsinghua University, Langfang, Hebei, 065001, People's Republic of China
[4] Collaborative Innovation Center of Quantum Matter, Beijing, 100084, People's Republic of China

E-mail: fliu@eng.utah.edu

Received 10 October 2018, revised 28 November 2018
Accepted for publication 23 January 2019
Published 20 February 2019

Abstract

A three-dimensional (3D) continuum percolation model has been developed on the basis of Monte Carlo simulation to investigate the percolation behavior of an electrically insulating matrix reinforced with multiple conductive fillers of different dimensionalities. Impenetrable fillers of large aspect ratio are found to preferentially align with each other to maximize the packing entropy rather than forming randomly oriented clusters. This entropy-driven transition from isotropic to nematic phase is shown to critically affect the percolation threshold. It suggests that an isotropic phase with a smaller nematic order parameter leads to a reduction in percolation threshold. In addition, a combination of two fillers with different dimensionalities can achieve a working concentration below the percolation threshold of single component system, which is further validated by the experiments of electrical conductivity in multicomponent multidimensional nanocarbon composites.

Supplementary material for this article is available online

Keywords: percolation, multicomponent nanocomposites, isotropic-nematic transition, graphene, carbon nanotubes

(Some figures may appear in colour only in the online journal)

1. Introduction

The intensive explorations of multicomponent composites have enabled their rapid developments in numerous structural engineering and functional applications [1–3]. Composites with enhanced electrical, mechanical and thermal performance can be fabricated by mixing polymer resins with high aspect ratio (AR) fillers [4, 5]. In particular, one-dimensional (1D) carbon nanotubes (CNTs) and 2D graphene nanoplatelets (GNPs) are attractive fillers for fabricating light-weight and high-performance nanocarbon composites [6, 7]. The formation of the conducting paths in the composites can in principle be explained by the percolation theory, [8] and the critical transition point from insulating to conductive is defined as percolation threshold. The significance of percolation transition lies in the fact that the percolating cluster formed by the conductive fillers at the percolation threshold immediately leads to a dramatic change in transport properties rather than following the linear rule of mixture. Many experimental efforts have been devoted to preparing multicomponent nanocarbon composites with lower percolation threshold and higher performance [2, 4, 9–15]. However, these experimental investigations were usually conducted on a trial-and-error basis without an in-depth understanding of

the percolation phenomena. Therefore, modeling of the electrical percolation is very essential to aid the experimental efforts by obtaining a comprehensive understanding of the mechanism of phase transition at the percolation threshold.

Up to date, only percolation models for single component composites (i.e. CNTs, [16–19] GNPs, [20–22] and carbon black, [23, 24]) have been well established, while the simulation of percolation phenomena in multicomponent composites is still at its infancy. One outstanding limitation of most existing models [25–28] is that they have not considered the alignment effect of nanofillers caused by the isotropic-nematic (*I–N*) phase transition. The alignment effect caused by entropy was first predicted in 1940 s by Onsager, [29] who showed that hard rods at high density should orient themselves in the same direction to maximize their freedom to translate. This entropic alignment is the origin of the *I–N* phase transition in liquid crystal, which has been also shown in the composites containing rod-like [29–31] and plate-like fillers [32–34]. There are also other limitations in the existing models. For instance, a discrete lattice was adopted to study the geometric percolation in the mixtures of isotropically oriented rods and disks, [25, 26] which should be more appropriately simulated as a continuum percolation problem. In some study, [27] the fillers were assumed to be soft-core to allow penetration between fillers for computational convenience, which cannot accurately describe the contact between the realistic fillers. Therefore, developing a more comprehensive 3D continuum percolation model is highly desirable to simulate the percolation phenomena in multicomponent composites, especially to evaluate the alignment effect caused by the *I–N* phase transition on the percolation threshold.

Here, we present a comprehensive analysis of the electrical percolation in multicomponent composites by developing a 3D percolation model on the basis of Monte Carlo simulations that removes some critical limitations in the previous models. Most importantly, we show that the entropy-driven *I–N* transition plays a critical role in determining the percolation threshold. Furthermore, an appropriate combination of 1D and 2D fillers can achieve a working concentration below the percolation threshold of single component system, which is further experimentally validated. Our work has provided new insights into the microstructural optimization of nanocarbon composites, which is expected to stimulate more interest and provide useful guidelines for experiments in the emerging field of multicomponent nanocomposites.

2. Simulation methods

Each filler in 3D space is determined by several variables. For example, 1D filler is identified by the center point, orientation angle and length, and 2D filler is identified by the center point, normal vector and radius, respectively. The center point of each filler is randomly selected inside the simulated box. Both the diameter of 2D filler and the length of 1D filler are set at unity. AR of 1D filler is defined as the ratio of its length to its diameter, and AR of 2D filler is the ratio of its diameter to its thickness, which defines the diameter of the 1D filler and the thickness of the 2D filler respectively. All the simulations were performed in a $10 \times 10 \times 10$ cubic box, i.e. its side dimensions are 10 times of the diameter of disk or length of stick. The orientation angle of 1D filler is the angle between the line containing the stick and x–y plane. The dihedral angle is the angle between the plane containing the 2D filler and x–y plane. The detailed generation procedures of fillers are described in the supplementary information (SI). The desired disks are added one by one such that the recently added disk does not overlap with the previously added ones. The procedure is continued until the end of trail loop or the end of the Monte Carlo loop is reached, as illustrated in Figure S1 is available online at stacks.iop.org/NANO/30/185302/mmedia in SI. The determination of the intersection between fillers is described in SI (see Figure S2). However, random sequential addition method suffers from a major drawback that for a given AR, there is a theoretical limit on the maximum volume fraction that can be obtained by finite random trials [20, 35]. As shown in Figure S3, 100 000 trials for 1000 desired fillers only successfully generate about 720 fillers averaged from 10 runs, which is below the percolation threshold. Therefore, we propose a more realistic model, consisting of disks with a hard and impenetrable core, surrounded by a soft cell, which acts as a buffer shell to allow for deformation. Two disks are connected if the distance between them was greater than the hard core diameter and less than the diameter of the core and soft shell together. Thus, percolation can happen before reaching the theoretical limit on the maximum volume density set by random sequential addition method.

The percolation cluster is determined by the well-known cluster labelling process [36] and has been adopted in our previous work of a 2D model [37]. Using this cluster labelling process, an algorithm is developed to graphically represent the 3D disk model (figures 1(a) and (b)) and 3D disk-stick model (figures 1(c) and (d)), respectively. AR of disk in figures 1(a) and (b) is 50 and the dihedral angle is 45°. The azimuthal angles of the normal vectors for disks are random distributed. The volume fraction in the case of figure 1(a) is 6.28 vol% with the density of four disks per unit volume. In figure 1(c), AR and dihedral angle of disk are kept the same as those in figure 1(a). The stick has AR of 20 and the same orientation angle as the dihedral angle of disk. The azimuthal angle for both sticks and disks are random distributed. In order to clearly represent the percolating phenomena in multicomponent system, the AR of stick used here to graphically represent the percolation phenomena in figures 1(c) and (d) is smaller than the value we used to investigate the percolation properties, since less sticks are required to reach the percolation limit. The volume fraction of multicomponent system in the case of figure 1(c) is 5.30 vol% with the density of three disks and three sticks per unit volume.

The alignment effect caused by the *I–N* phase transition in 3D disk model is considered. The nematic order parameter (S) [38] is used to represent the overall alignment of the disks,

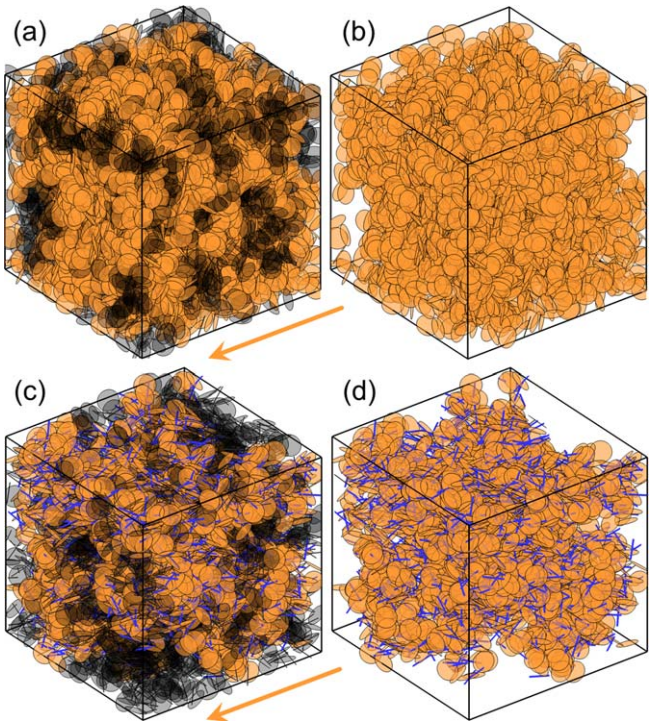

Figure 1. Graphic representations of 3D percolation model. (a) 3D disk model with black finite clusters and orange percolating cluster. (b) Percolating cluster in (a). (c) 3D disk-stick model with black finite clusters, and percolating cluster with orange disks and blue sticks. (d) Percolating cluster in (c). The arrow indicates the percolating direction. The diameter of disk and the length of stick are set at unity, and ARs for disk and stick are 50 and 20, respectively.

which is given by the largest eigenvalue of Q,

$$Q = \frac{1}{2N}\sum_{i}^{N}(3\overrightarrow{n_i}\overrightarrow{n_i} - I), \tag{1}$$

where N is the total number of disks, $\vec{n}$ is the normal vector, and $\boldsymbol{I}$ is the identity matrix. In a fully aligned configuration, $S = 1$; in a perfectly isotropic configuration, $S = 0$.

3. Results and discussion

Firstly, the nematic order parameter as a function of dihedral angle is investigated focusing on the effect of the *I–N* phase transition on percolation threshold in composites with only 2D fillers. Then, the synergistic effect in multicomponent composites is obtained and the simulation results are further validated by the experiments. Many experiments and simulations on variously shaped hard particles have revealed the entropy-driven transitions, [34, 39, 40] which are the origin of *I–N* transition in a liquid crystal. For 2D fillers, the normal vector, $\vec{n}$, is not restricted by the center point and its polar angle is complementary to the dihedral angle, as shown in figure 2(a). One can imagine that all the normal vectors with the same value of polar angle start from the same point and scatter into different directions in 3D space and each of them can be represented by a lateral edge of a cone, as indicated by the red arrow in figure 2(a). When disks are all parallel to the x–y plane with $\vec{n}$ pointing along z-axis, S has the largest value of 1, indicating the formation of a perfectly ordered phase. When disks are perpendicular to the x–y plane, S has a small value around 0.3, indicating a relatively disordered phase with $\vec{n}$ randomly orientated in x–y plane. The steradian of the cone varies with the dihedral angle, similar to closing or fully opening an umbrella with $\vec{n}$ as its rib, which corresponds to the above described two extreme cases, respectively.

The Monte Carlo simulation results of the nematic order parameter as a function of dihedral angle are shown in figure 2(b), where each data point is averaged from 10 runs. In the simulation, the disks are generated with randomly distributed center points and fixed dihedral angle. The azimuthal angle of normal vector is a random value in the range of $(0, 2\pi)$. In other word, the normal vectors of disks isotropically rotate in the x–y plane even though the polar angle stays the same for each data point. The nematic order parameter is the largest eigenvalue of Q, which can be calculated by equation (1). The value of S initially decreases with the increase of the dihedral angle in the range of 15°–50°, and then turns around to slightly increasing as the dihedral angle goes from 60° to 75°. With a small dihedral angle, disks are nearly parallel to the x–y plane representing an ordered phase. Consequently, S has a large value, close to 1. In contrast, with a large dihedral angle close to 90°, disks rotate along z-axis, leading to a relatively isotropic phase with a small S value, less than 0.3 but still larger than 0. The normal vectors are parallel to z-axis with the dihedral angle of 0° and perpendicular to z-axis with the dihedral angle of 90°. One can expect that there is a critical value of dihedral angle, Φ_c, between 0° and 90°, and S decreases from one to some small value, S_c, in the range of (0°, Φ_c) and then increases from S_c to 0.3 in the range of (Φ_c, 90°). With the finite number of disks generated in each run, the calculated transition point, S_c is in the vicinity of 55°, as shown in figure 2(b). It is not possible in the simulations to exactly locate the value of Φ_c owing to the finite simulation times, but a numerical analysis of the relationship between S and the dihedral angle according to equation (1) can be carried out to derive Φ_c exactly.

The cross product in equation (1) is

$$\overrightarrow{n_i}\overrightarrow{n_i} = \begin{bmatrix} \sin^2\theta\sin^2\varphi & \sin\theta\cos\theta\sin^2\varphi & \sin\theta\sin\varphi\cos\varphi \\ \sin\theta\cos\theta\sin^2\varphi & \cos^2\theta\sin^2\varphi & \cos\theta\sin\varphi\cos\varphi \\ \sin\theta\sin\varphi\cos\varphi & \cos\theta\sin\varphi\cos\varphi & \cos^2\varphi \end{bmatrix}. \tag{2}$$

When the number of disks, N, approaches the infinity and θ is randomly distributed in the range of $(0, 2\pi)$, equation (2) can be simplified as,

$$Q = \begin{bmatrix} \frac{3}{4}\sin^2\varphi - \frac{1}{2} & 0 & 0 \\ 0 & \frac{3}{4}\sin^2\varphi - \frac{1}{2} & 0 \\ 0 & 0 & \frac{3}{2}\cos^2\varphi - \frac{1}{2} \end{bmatrix}. \tag{3}$$

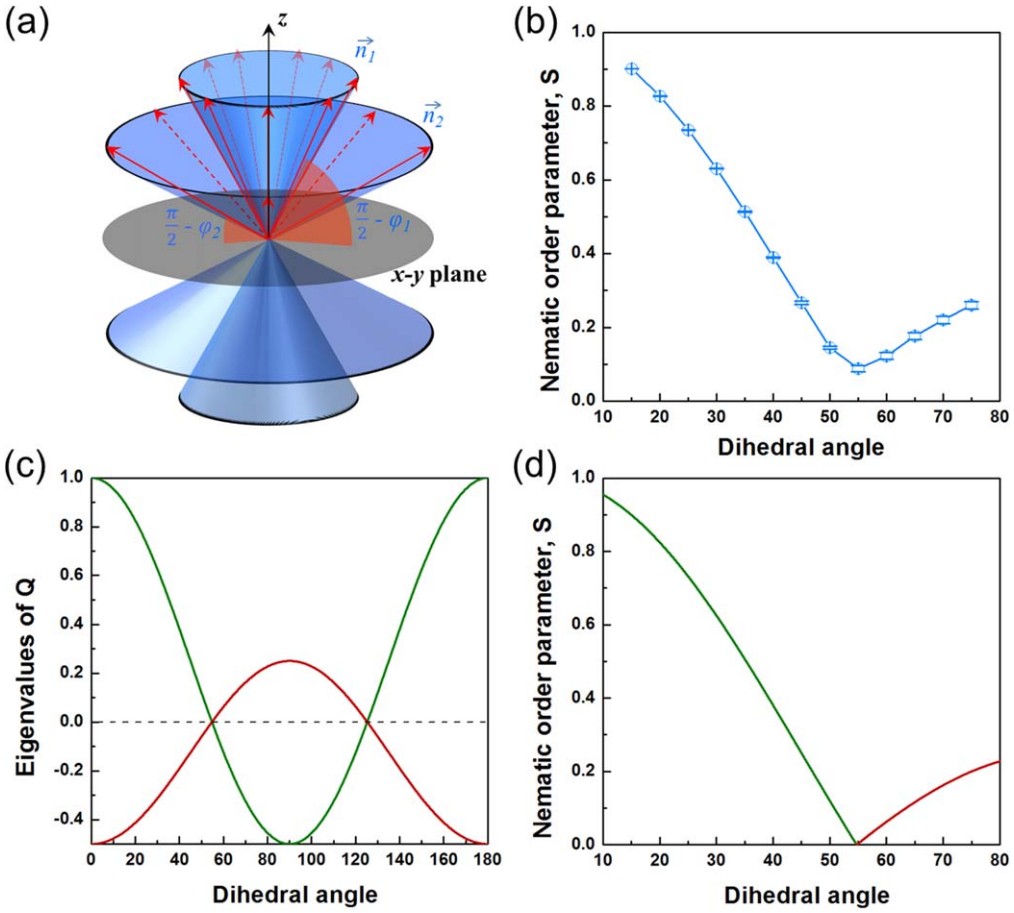

Figure 2. (a) Schematic illustration of the nematic order parameter as a function of dihedral angle. (b) Simulation results of nematic order parameter as a function of dihedral angle averaged from 10 runs. (c) Dependencies of eigenvalues of Q (a) and nematic order parameter (b) on dihedral angle from equation (4). Red color represents $\frac{3}{4}\sin^2\varphi-\frac{1}{2}$ and green color represents $\frac{3}{2}\cos^2\varphi-\frac{1}{2}$, respectively.

It is straightforward to obtain S as the largest eigenvalue of Q.

$$\mathrm{Eig}(Q)=\frac{3}{4}\sin^2\varphi-\frac{1}{2};\ \frac{3}{4}\sin^2\varphi-\frac{1}{2};\ \frac{3}{2}\cos^2\varphi-\frac{1}{2} \quad (4)$$

In order to expedite the simulation of the effect of nematic order on percolation phenomena, simulation results with a fixed dihedral angle are compared with those with dihedral angle varying around the fixed value over a selected range. The percolation probability as a function of density

$$S=\max(\mathrm{Eig}(Q))=\begin{cases}\dfrac{3}{4}\sin^2\varphi-\dfrac{1}{2};\ \cos^{-1}\left(\dfrac{\sqrt{3}}{3}\right)<\varphi<\cos^{-1}\left(-\dfrac{\sqrt{3}}{3}\right)\\ \dfrac{3}{2}\cos^2\varphi-\dfrac{1}{2};\ 0<\varphi<\cos^{-1}\left(\dfrac{\sqrt{3}}{3}\right)\text{ and }\cos^{-1}\left(-\dfrac{\sqrt{3}}{3}\right)<\varphi<\pi\end{cases}. \quad (5)$$

Equations (4) and (5) are plotted in figures 2(c) and (d), respectively. There is a very good agreement between the numerical and simulation results. Initially, S decreases with the increasing dihedral angle and then slowly increases as the dihedral angle approaches 90°. The value of Φ_c from the numerical analysis is $\cos^{-1}(\sqrt{3}/3)\approx 54.74°$, which defines the transition point ($S=0$). Thus, by modulating the dihedral angle, one can effectively tune the value of S to achieve different phases.

was carried out for two specified dihedral angle ranges: (20°, 30°) and (35°, 45°), respectively. As shown in Figure S4 in SI, there are no significant differences for percolation probability between an angle range (dihedral angle ±5°) and fixed dihedral angle (dihedral angle = 25° in Figure S4(a) and 40° in Figure S4(b)). Therefore, a single dihedral angle value was adopted to investigate how the *I–N* phase transition will affect the percolation threshold in the following study. In composites with high AR fillers, the *I–N* phase transition has been

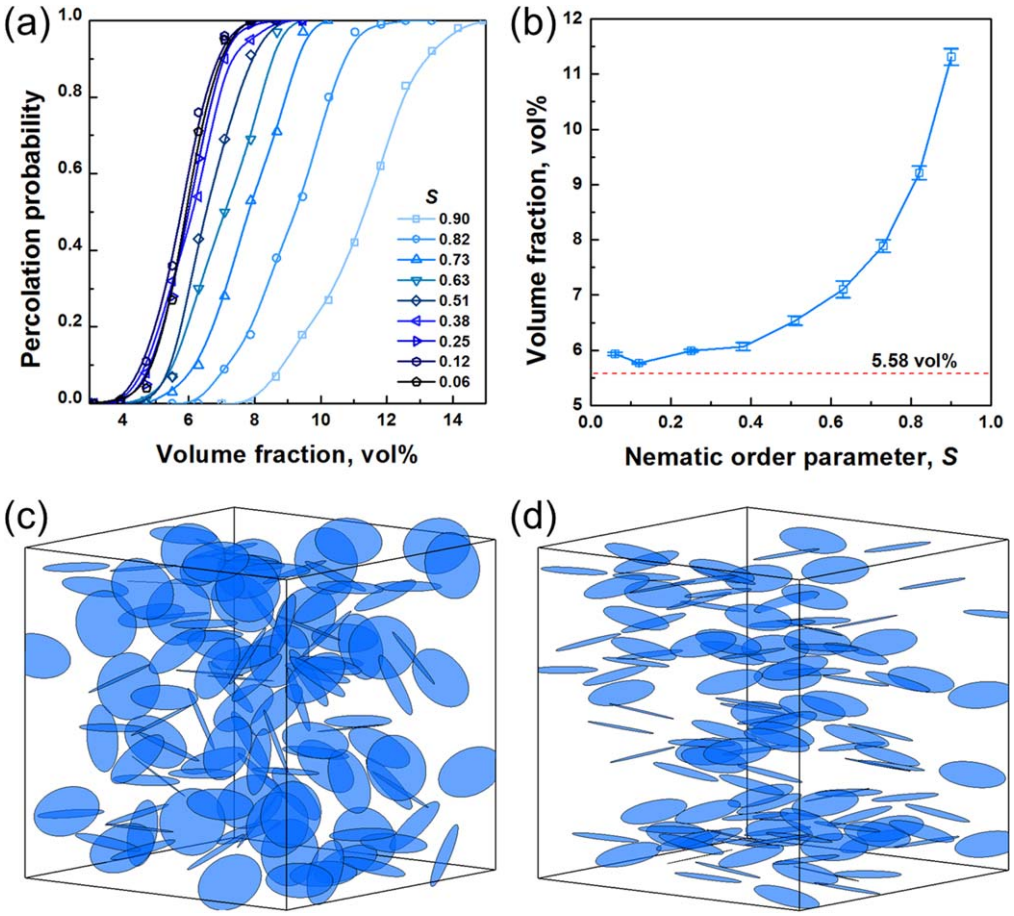

Figure 3. (a) Percolation probability as a function of volume fraction for different nematic order parameters. (b) Volume fraction at percolation threshold as a function of nematic order parameters. The red dashed line indicates the threshold for the system with randomly distributed disks. Graphic representations of disks without (c) and with nematic orientational order (d).

found to preempt the percolation transition [40]. Therefore, a strong dependence of the percolation threshold on S is expected. With the increasing order of alignment (the increasing value of S), the intersection between disks is adversely affected, leading to an increase of the percolation threshold. When the value of S varies from 0.06 to 0.90, there is salient right-shift of the percolation probability curves, as depicted in figure 3(a). This indicates an increase of the percolation threshold with the entrance of the nematic phase. In all the cases, AR of 50 is adopted for the 2D filler. Each data point represents the percolation probability as the ratio of percolated times to the total number of simulations performed and a spline fitted solid-line curve is used to derive the percolation threshold, which is the inflection point. The same analysis method is adopted for the following investigation.

The obtained percolation threshold values in volume fraction are shown in figure 3(b). With the increasing value of S from 0.06 to 0.90, there is an increase in the critical volume fraction. When fillers with high AR become highly aligned with larger value of S, fewer bridges exist between them and the percolation network no longer survives. This results in a substantial drop in the observable data, such as electrical conductivity and thermal conductivity [17, 41, 42]. When S has a small value less than 0.4, representing a relatively isotropic phase, the percolation threshold approaches a plateau, which is close to the value of the threshold (5.58 vol%) in the system with randomly oriented disks. Figures 3(c) and (d) show the graphic representations of disks without and with nematic orientational order, respectively. The density of disk is adopted as one disk/unit volume for both cases. The phase with decreased S value facilitates the formation of the percolation network, which can effectively reduce the percolation threshold. Thus, the alignment of fillers has a significant effect on the percolation threshold and the *I–N* transition can lead to an increase of the volume fraction to form the percolating path.

The effect of AR on the percolation threshold is also investigated with the isotropically oriented 2D fillers. As depicted in figure 4(a), the solid-line curves of percolation probability shift to the left with the increase of AR from 40 to 500. As derived from the percolation probability curves, the percolation thresholds predicted for different ARs show an inversely proportional relationship as $\varnothing_c = 2.83/\mathrm{AR}$, which is represented in figure 4(b). The insert shows the volume fraction as a function of the reciprocal of AR, which is obviously a linear relationship with the fitted coefficient 2.83 ± 0.03. AR is determined by the ratio of the diameter to the thickness for 2D filler, which has a smaller dimension for thin 2D filler with high AR. The thickness of 2D filler becomes negligible with respect

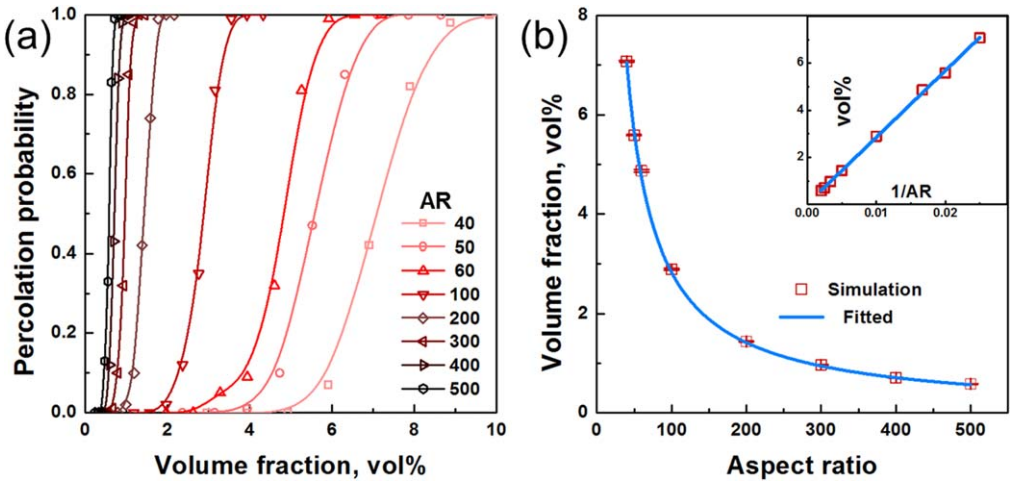

Figure 4. (a) Percolation probability as a function of volume fraction for different ARs (AR: 40–500). (b) Volume fraction at percolation threshold as a function of AR. The insert shows the volume fraction as a function of the reciprocal of AR (1/AR) with a linear relationship.

to the diameter. Within the given range (40–500), the variation of the thickness has an insignificant influence on the critical density. As shown in Figure S5(a) in SI, the curves of percolation probability as a function of density for different ARs almost overlap with each other and the derived critical density does not change significantly.

The volume fraction at the percolation threshold (in figure 4(b)) determined by the product of the critical density and unit volume is inversely proportional to AR, which is consistent with the previous studies [27, 43]. The volume fraction, $\varnothing_c$, at the percolation threshold is calculated by

$$\varnothing_c = D_c \times \frac{\pi d^2}{4} \times \frac{d}{\mathrm{AR}}, \tag{6}$$

where D_c is the density of fillers at the percolation threshold and d is the diameter of 2D disk. From the Monte Carlo simulation results, D_c can be approximately treated as a constant (see Figure S5(b)). Under this assumption, the critical volume fraction can be considered as a function of only AR in equation (6), resulting in an inversely proportional relationship with the coefficient of $\pi d^3 D_c/4$. By using the fitted coefficient value of 2.83 ± 0.03 and $d = 1$, one can obtain the value of D_c as 3.60 ± 0.04 disks per unit volume, which is represented by the blue line in Figure S4(b). By doing the numerical analysis, we have a fairly clear picture of the inversely proportional relationship between volume fraction and AR. This confirms that a higher AR of 2D fillers can lead to a lower percolation threshold.

Next, we investigate the synergistic effect in hybrid systems. Previous studies have shown that the dispersion of CNTs in polymer can have a significant influence on the percolation threshold [43, 44]. Agglomeration and unsuccessful dispersion of CNTs in experiments are very likely to take place and challenging to capture in simulations [45]. And also it is hard to achieve the extremely low percolation threshold in experiments as estimated by simulations for polymers reinforced with only CNTs. For these reasons, the pure 1D stick model is not considered in this study. Instead, we take the advantage of relatively uniform distribution of 2D

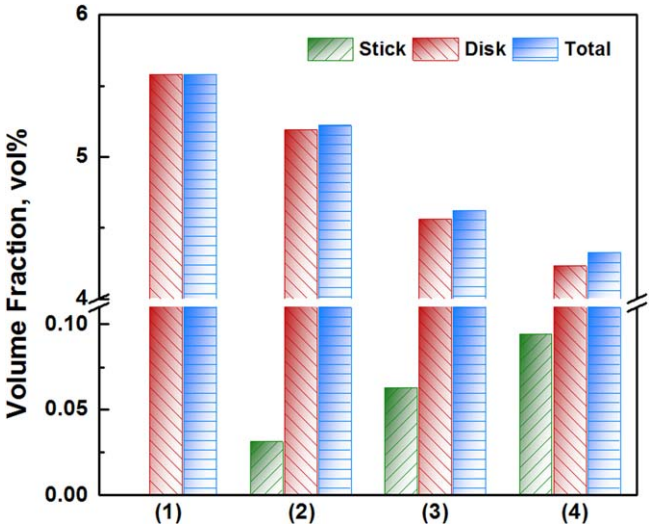

Figure 5. Distribution of volume fraction at the percolation threshold in four scenarios with the increasing number of sticks per unit volume in sequence: (1) no stick added, (2) one stick/unit volume, (3) two sticks/unit volume, and (4) three sticks/unit volume, respectively.

fillers in polymer-based composites, and randomly add 1D fillers into the isotropically oriented 2D disk system to see how the critical volume fraction changes. In the simulation, both disk and stick have AR of 50. Figure 5 shows four scenarios with the addition of 1D fillers in sequence: (1) no stick added, (2) one stick/unit volume, (3) two sticks/unit volume, and (4) three sticks/unit volume, respectively. The total volume fraction at the percolation threshold is found to decrease continuously from 5.58 to 5.22, 4.62 and 4.33 vol%, which clearly demonstrates a reduction of the total volume fraction. The simulation results of hybrid disk-stick percolation model suggest that the percolation threshold of 2D fillers can be substantially lowered by adding small quantities of 1D fillers into the composites. The trend of the volume fraction at the percolation threshold predicted by the presented method for hybrid systems is consistent with the synergistic effect

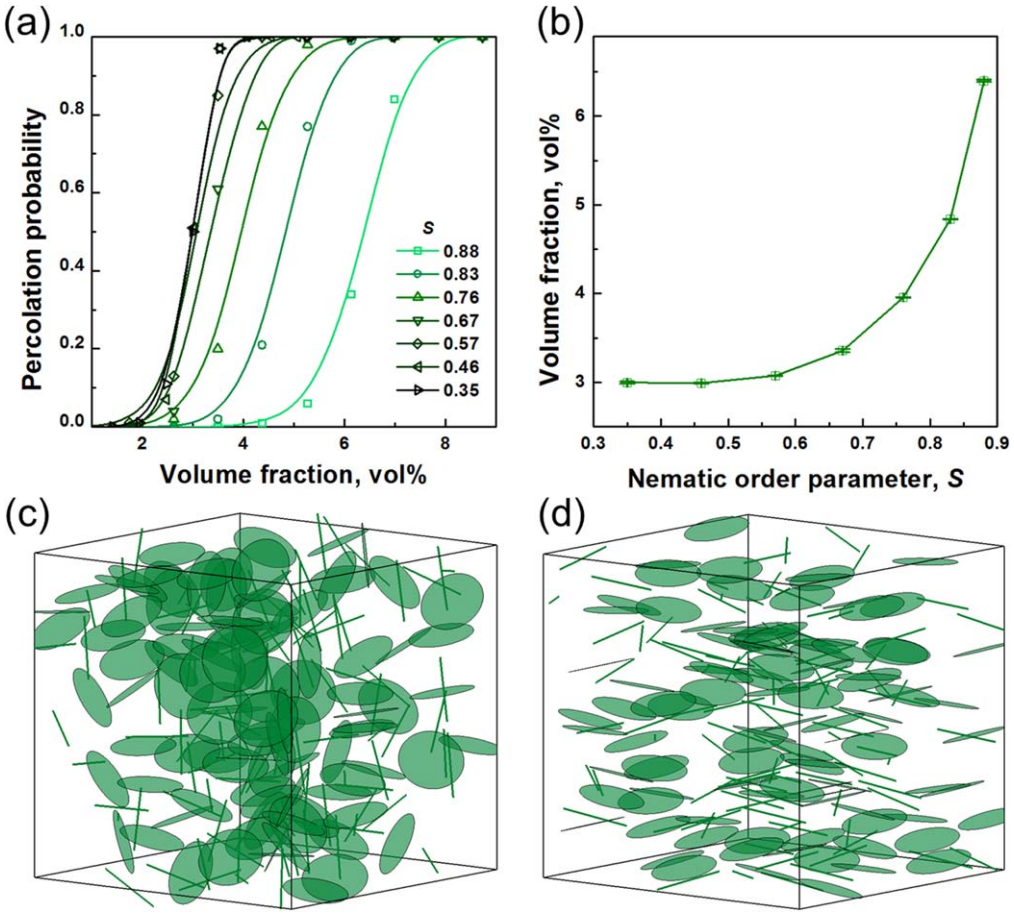

Figure 6. In a hybrid system of 90 vol% 2D disk and 10 vol% 1D stick, (a) percolation probability as a function of volume fraction for different nematic order parameters and (b) volume fraction at percolation threshold as a function of nematic order parameter. Graphic representations of fillers in hybrid systems without (c) and with (d) nematic orientational order.

observed by the experimental and theoretical studies [12, 46, 47].

As elaborated above, the alignment effect caused by the *I–N* phase transition plays a critical role in determining the percolation threshold in pure 2D system. The same trend is also observed in the hybrid systems. In the simulation, the volume fractions of 2D and 1D fillers are held constant as 90 vol% and 10 vol% and AR is adopted as 50 for both disk and stick. The percolation threshold is found to decrease with the increase of the orientation angle of 1D filler and the dihedral angle of 2D filler. The percolation probability with respect to *S* is shown in figure 6(a). As the value of *S* changes from 0.35 to 0.88, a right-shift of the percolation probability curve is observed and the derived percolation threshold decreases accordingly, as depicted in figure 6(b). Similar to the pure disk percolation model, the isotropic phase with a smaller value of *S* leads to a lower total volume fraction to reach the percolation limit than the nematic phase. Figures 6(c) and (d) show the graphic representations of fillers in hybrid systems without and with nematic orientational order. The density of disk is chosen as 0.8 disks/unit volume and the density of stick is 0.8 sticks/unit volume for clarity in both cases. In an isotropic phase, there are more contacts between fillers than in nematic phase, so that the randomly orientated fillers facilitate the formation of percolating cluster. In multicomponent composites, an appropriate combination of different fillers with different dimensionalities and proper degree of orientation can entice a significant reduction in the critical volume fraction.

Finally, the simulation results in multicomponent system have been validated by experiments. Eight samples were prepared using multi-walled CNTs as the 1D fillers and GNPs as 2D fillers. At each composition, one material consists of only 2D GNPs, while the other contains 10 vol% 1D CNTs and 90 vol% 2D GNPs, respectively. Generally, morphology and distribution of fillers in a polymer matrix have significant effects on the composite properties. Figure S6 shows the dispersion of nanocarbon fillers in the polymer matrix observed under SEM. The electrical conductivity was calculated from the thickness and the sheet resistance measurements. The detailed experimental method is described in SI. Figure 7(a) shows the electrical conductivity in two samples as a function of volume fraction. The hybrid sample with 90 vol% GNPs and 10 vol% CNTs distinctly has a higher conductivity and lower percolation threshold than the sample with pure 2D GNPs. The synergistic effects observed in experimental studies are linked closely with the incremental contacts between these nanocarbon fillers and thus improves the current flow through the percolation path to enhance the electrical conductivity.

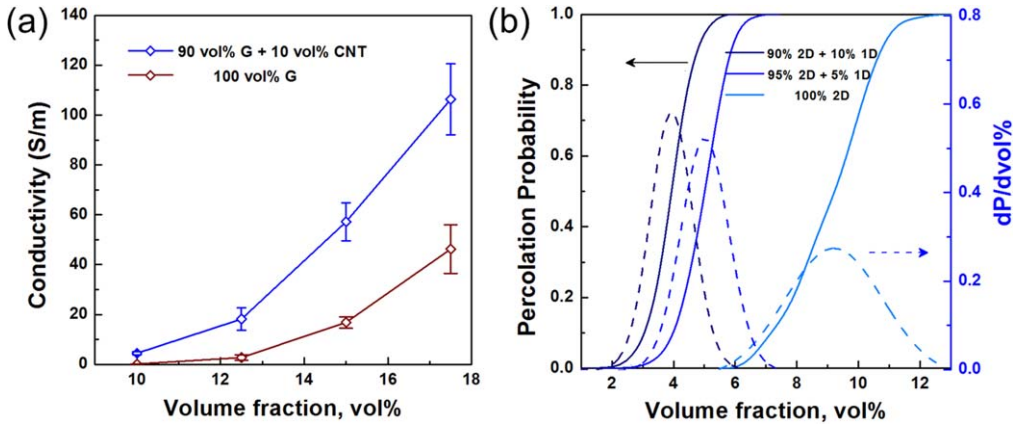

Figure 7. Comparison between experiment (a) and simulation (b).

As we demonstrated in the previous study [37], there is a synergistic effect when two components are combined properly, which will not only reduce the materials consumption but also enhance the electrical conductivity of the composites. In the experiments, all the samples are prepared as thin films, which indicate that all the fillers are likely to incline towards the *x*–*y* plane. Therefore, both the orientation angle of 1D stick and the dihedral angle of 2D disk in this simulation are selected with a small value as 20° and AR is adopted as 50. The simulation results of percolation probability of fillers with different volume percentage are shown in figure 7(b). Each dashed line is the first-order derivative of percolation probability, which is used to derive the percolation threshold. The pure system with only 2D fillers has a higher critical volume fraction than the hybrid system. The volume fraction at the percolation threshold dramatically decreases from 9.21 to 5.26 and 3.94 vol% after replacing 5 vol% and 10 vol% 2D disks with 1D sticks, respectively. Thus, gradually replacing 2D disks with an equivalent volume of 1D sticks can significantly reduce the percolation threshold. The trend of the percolation threshold in simulation results is consistent with that in the experimental observation on conductivity. The presented 3D disk-stick percolation model can provide an effective way to evaluate the synergistic effect in hybrid composites incorporating multiple nanocarbon fillers with different dimensionalities.

4. Conclusions

In summary, a 3D continuum percolation model has been developed on the basis of Monte Carlo simulation, which is able to predict the electrical percolation threshold of multicomponent multidimensional composites. This proposed 3D percolation model can account for both the alignment effect and shape effect of different fillers to overcome the limitation of previous work. The entropy-driven phase transition from isotropic to nematic suggests that a smaller degree of fillers' orientation with a larger nematic order parameter leads to an increase in percolation threshold. Also, high AR leads to a reduction of the critical volume fraction. For multicomponent nanocarbon composites, there is a synergistic effect leading to a lower working concentration than single component system when two fillers of different dimensionalities are combined properly. Our simulation results can provide an effective pathway to the design of multicomponent multidimensional composites, which can serve as the guidance for experimental studies.

Acknowledgments

We acknowledge the financial support from DOE-BES (No. DE-FG02-04ER46148) and Life-E LLC in Salt Lake City, UT. We also thank NERSC and CHPC at the University of Utah for providing the computing resources.

ORCID iDs

Xiaojuan Ni https://orcid.org/0000-0002-5845-7404

References

[1] Kim K K, Hong S, Cho H M, Lee J, Suh Y D, Ham J and Ko S H 2015 Highly sensitive and stretchable multidimensional strain sensor with prestrained anisotropic metal nanowire percolation networks *Nano Lett.* **15** 5240–7
[2] Seo H, Yun H D, Kwon S-Y and Bang I C 2016 Hybrid graphene and single-walled carbon nanotube films for enhanced phase-change heat transfer *Nano Lett.* **16** 932–8
[3] Zhang C J *et al* 2017 Enabling flexible heterostructures for li-ion battery anodes based on nanotube and liquid-phase exfoliated 2d gallium chalcogenide nanosheet colloidal solutions *Small* **13** 1–11
[4] Yu A, Ramesh P, Sun X, Bekyarova E, Itkis M E and Haddon R C 2008 Enhanced thermal conductivity in a hybrid graphite nanoplatelet-Carbon nanotube filler for epoxy composites *Adv. Mater.* **20** 4740–4
[5] He G, Zhou X, Liu J, Zhang J, Pan L and Liu S 2017 Synergetic enhancement of thermal conductivity for highly explosive-filled polymer composites through hybrid carbon nanomaterials *Polym. Compos.* **39** 1–11

[6] Zhang D, Ryu K, Liu X, Polikarpov E, Ly J, Tompson M E and Zhou C 2006 Transparent, conductive, and flexible carbon nanotube films and their application in organic light-emitting diodes *Nano Lett.* **6** 1880–6

[7] Gomez De Arco L *et al* 2010 Continuous, highly flexible, and transparent graphene films by chemical vapor deposition for organic photovoltaics *ACS Nano* **4** 2865–73

[8] Stauffer D and Aharony A 1992 *Introduction to Percolation Theory* (London: Taylor and Francis)

[9] Kim T, Park J, Sohn J, Cho D and Jeon S 2016 Bioinspired, highly stretchable, and conductive dry adhesives based on 1d-2d hybrid carbon nanocomposites for all-in-one ecg electrodes *ACS Nano* **10** 4770–8

[10] Kholmanov I N *et al* 2012 Improved electrical conductivity of graphene films integrated with metal nanowires *Nano Lett.* **12** 5679–83

[11] Yu J, Choi H K, Kim H S and Kim S Y 2016 Synergistic effect of hybrid graphene nanoplatelet and multi-walled carbon nanotube fillers on the thermal conductivity of polymer composites and theoretical modeling of the synergistic effect *Composites* A **88** 79–85

[12] Yue L, Pircheraghi G, Monemian S A and Manas-zloczower I 2014 Epoxy composites with carbon nanotubes and graphene nanoplatelets-Dispersion and synergy effects *Carbon* **78** 268–78

[13] Safdari M and Al-Haik M S 2013 Synergistic electrical and thermal transport properties of hybrid polymeric nanocomposites based on carbon nanotubes and graphite nanoplatelets *Carbon* **64** 111–21

[14] Chatterjee S, Nafezarefi F, Tai N H, Schlagenhauf L, Nüesch F A and Chu B T T 2012 Size and synergy effects of nanofiller hybrids including graphene nanoplatelets and carbon nanotubes in mechanical properties of epoxy composites *Carbon* **50** 5380–6

[15] Ahn Y, Jeong Y, Lee D and Lee Y 2015 Copper nanowire-graphene core–shell nanostructure for highly stable transparent conducting electrodes *ACS Nano* **9** 3125–33

[16] Zeng X, Xu X, Shenai P M, Kovalev E, Baudot C, Mathews N and Zhao Y 2011 Characteristics of the electrical percolation in carbon nanotubes/polymer nanocomposites *J. Phys. Chem.* C **115** 21685–90

[17] Mutiso R M and Winey K I 2015 Electrical properties of polymer nanocomposites containing rod-like nanofillers *Prog. Polym. Sci.* **40** 63–84

[18] Celzard A, McRae E, Deleuze C and Dufort M 1996 Critical concentration in percolating systems containing a high-aspect-ratio filler *Phys. Rev.* B **53** 6209–14

[19] Kyrylyuk A V and van der Schoot P 2008 Continuum percolation of carbon nanotubes in polymeric and colloidal media *Proc. Natl Acad. Sci. USA* **105** 8221–6

[20] Kale S, Sabet F A, Jasiuk I and Ostoja-Starzewski M 2015 Tunneling-percolation behavior of polydisperse prolate and oblate ellipsoids *J. Appl. Phys.* **118** 1–9

[21] Li J and Kim J 2007 Percolation threshold of conducting polymer composites containing 3D randomly distributed graphite nanoplatelets *Compos. Sci. Technol.* **67** 2114–20

[22] Mutlay I and Tudoran L B 2014 Percolation behavior of electrically conductive graphene nanoplatelets/polymer nanocomposites: theory and experiment *Fullerenes Nanotub. Carbon Nanostructures* **22** 413–33

[23] Balberg I 2002 A comprehensive picture of the electrical phenomena in carbon black-polymer composites *Carbon* **40** 139–43

[24] Huang J C 2002 Carbon black filled conducting polymers and polymer blends *Adv. Polym. Technol.* **21** 299–313

[25] Chatterjee A P 2015 A lattice model for connectedness percolation in mixtures of rods and disks *J. Phys. Condens. Matter* **27** 1–7

[26] Xiong Z Y, Zhang B Y, Wang L, Yu J and Guo Z X 2014 Modeling the electrical percolation of mixed carbon fillers in polymer blends *Carbon* **70** 233–40

[27] Chen Y, Pan F, Wang S, Liu B and Zhang J 2015 Theoretical estimation on the percolation threshold for polymer matrix composites with hybrid fillers *Compos. Struct.* **124** 292–9

[28] Kale S, Karimi P, Sabet F A, Jasiuk I and Ostoja-starzewski M 2018 Tunneling-percolation model of multicomponent nanocomposites *J. Appl. Phys.* **123** 1–12

[29] Onsager L 1949 The effects of shape on the interaction of colloidal particles *Ann. New York Acad. Sci.* **51** 627–59

[30] Flory P J 1956 Phase equilibria in solutions of rod-like particles *Proc. R. Soc.* A **234** 73–89

[31] Nigro B and Grimaldi C 2014 Impact of tunneling anisotropy on the conductivity of nanorod dispersions *Phys. Rev.* B **90** 1–14

[32] Van Der Kooij F M, Kassapidou K and Lekkerkerker H N W 2000 Liquid crystal phase transitions in suspensions of polydisperse plate-like particles *Nature* **406** 868–71

[33] Vroege G J and Lekkerkerker H N W 1992 Phase transitions in lyotropic liquid crystals *Rep. Prog. Phys.* **55** 1241–1309

[34] Yuan J, Luna A, Neri W, Zakri C, Schilling T, Colin A and Poulin P 2015 Graphene liquid crystal retarded percolation for new high-k materials *Nat. Commun.* **6** 1–8

[35] Sherwood J D 1997 Packing of spheroids in three-dimensional space by random sequential addition *J. Phys. A: Math. Gen.* **30** L839–43

[36] Hoshen J and Kopelman R 1976 Percolation and cluster distribution: I. Cluster multiple labeling technique and critical concentration algorithm *Phys. Rev.* B **14** 3438–45

[37] Ni X, Hui C, Su N, Jiang W and Liu F 2018 Monte Carlo simulations of electrical percolation in multicomponent thin films with nano fillers *Nanotechnology* **29** 1–10

[38] De G P G and Prost J 1993 *The Physics of Liquid Crystals* (New York: Oxford University Press)

[39] Manoharan V N 2015 Colloidal matter: packing, geometry, and entropy *Science* **349**

[40] Mathew M, Schilling T and Oettel M 2012 Connectivity percolation in suspensions of hard platelets *Phys. Rev.* E **85** 1–7

[41] Schilling T, Jungblut S and Miller M A 2007 Depletion-induced percolation in networks of nanorods *Phys. Rev. Lett.* **98** 1–4

[42] Potts J R, Dreyer D R, Bielawski C W and Ruoff R S 2011 Graphene-based polymer nanocomposites *Polymer* **52** 5–25

[43] Li J, Ma P C, Chow W S, To C K, Tang B Z and Kim J 2007 Correlations between percolation threshold, dispersion state, and aspect ratio of carbon nanotubes *Adv. Funct. Mater.* **17** 3207–15

[44] Bryning M B, Islam M F, Kikkawa J M and Yodh A G 2005 Very low conductivity threshold in bulk isotropic single-walled carbon nanotube-epoxy composites *Adv. Mater.* **17** 1186–91

[45] Ma P C, Mo S Y, Tang B Z and Kim J K 2010 Dispersion, interfacial interaction and re-agglomeration of functionalized carbon nanotubes in epoxy composites *Carbon* **48** 1824–34

[46] Oh J Y, Jun G H, Jin S, Ryu H J and Hong S H 2016 Enhanced electrical networks of stretchable conductors with small fraction of carbon nanotube/graphene hybrid fillers *ACS Appl. Mater. Interfaces* **8** 3319–25

[47] Liu H, Gao J, Huang W, Dai K, Zheng G, Liu C, Shen C, Yan X, Guo J and Guo Z 2016 Electrically conductive strain sensing polyurethane nanocomposites with synergistic carbon nanotubes and graphene bifillers *Nanoscale* **8** 12977–89